






RESEARCH ARTICLE | FEBRUARY 07 2023

Thin-film (Al)BCN materials synthesized by sequential precursor pulses to mimic atomic layer deposition

Ramazan O. Apaydin ; Antonius A. I. Aarnink; Dirk J. Gravesteijn ; Michel P. de Jong ; Alexey Y. Kovalgin  



AIP Advances 13, 025237 (2023)
<https://doi.org/10.1063/6.0002331>

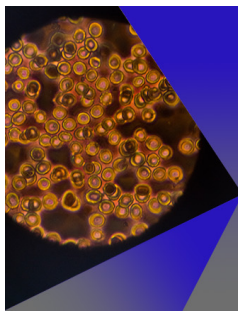


View
Online



Export
Citation

CrossMark



AIP Advances

Special Topic: Medical Applications
of Nanoscience and Nanotechnology

Submit Today!

Thin-film (Al)BCN materials synthesized by sequential precursor pulses to mimic atomic layer deposition

Cite as: AIP Advances 13, 025237 (2023); doi: 10.1063/6.0002331

Submitted: 6 December 2022 • Accepted: 16 January 2023 •

Published Online: 7 February 2023





View Online



Export Citation



CrossMark

Ramazan O. Apaydin,  Antonius A. I. Aarnink, Dirk J. Gravesteijn,  Michel P. de Jong, 
and Alexey Y. Kovalgin^{a)} 

AFFILIATIONS

MESA+ Institute for Nanotechnology, University of Twente, P.O. Box 217, 7500 AE, Enschede, The Netherlands

^{a)} Author to whom correspondence should be addressed: a.y.kovalgin@utwente.nl

ABSTRACT

This work brings novel insights into the existing knowledge on the deposition of films containing boron (B), carbon (C), nitrogen (N), and aluminum (Al). The (Al)BCN films are obtained at low substrate temperatures (T_S) of 250–400 °C from triethylborane, ammonia (NH₃), and trimethylaluminum. For BCN films, a nearly similar elemental composition of B_{0.42}C_{0.41}N_{0.15}O_{0.02}, with 1–2 at. % variations, is observed for substantial ranges of T_S and NH₃-exposure time. This can indicate a similar growth mechanism and/or formation of a single-phase material. While excluding precursor underdosing, a remarkable dependence of growth rate per cycle (GPC) on total gas pressure (P_{tot}) is observed. The GPC approaches near saturation regime for P_{tot} between 1 and 10 mbar, for $T_S = 330$ –375 °C, which might support the occurrence of a surface-adduct assisted pathway. The level of GPC saturation is influenced by T_S . For a wide range of process conditions, N-share in the films slightly varies between 12 and 16 at. %. C-share only changes between 40 and 42 at. %. The attempt to increase N-share by dissociating NH₃ into NH₂ radicals by hot wire assistance remarkably shows the opposite effect, i.e., a decrease in the N-share from 15 to 6 at. %. This is accompanied by a corresponding increase in the B- and, in particular, C-shares, suggesting that the removal of carbon can occur via the incorporation of nitrogen. For AlBCN films, changing P_{tot} has a strong effect on their elemental composition. At $P_{tot} = 10$ mbar, Al-deficient films grow, whereas a P_{tot} of 0.2 mbar leads to mainly AlN-containing films with some inclusions of BN.

© 2023 Author(s). All article content, except where otherwise noted, is licensed under a Creative Commons Attribution (CC BY) license (<http://creativecommons.org/licenses/by/4.0/>). <https://doi.org/10.1063/6.0002331>

I. INTRODUCTION

The family of boron (B), nitrogen (N), and carbon (C) containing materials exhibits a variety of attractive optical, electronic, and chemical properties, showing an example of the possibility to combine several functionalities in one compound.^{1–4} Graphene, hexagonal boron nitride (*h*-BN), and sp²-hybridized boron–carbon–nitrogen (BCN) composites exhibit near-perfect match of their crystal lattices.^{5–7} Layered BCN materials with composition ideally varying from pure graphene to pure *h*-BN are expected to have a rich variety of electronic and optical properties, notably a tunable bandgap and refractive index, potentially enabling new applications. For example, the optical bandgap of BCN was reported to increase for a higher nitrogen and lower carbon share.⁸ Therefore, synthesis, characterization, and possible applications of

BCN materials have been widely studied, both experimentally^{9–14} and theoretically.^{15–19} Importantly, carbon and *h*-BN tend to form segregated C- and BN domains in BCN, making the formation of single-phase BCN films challenging. Although these materials are generally united under the term “BCN” in the literature, their constituting phases are usually not well specified. Applying high-temperature processes will more likely lead to the separation of phases since this is thermodynamically favorable.^{8,17} Synthesizing a single-phase BCN film might benefit from applying low-temperature methods.

This work aims to bring the following novel aspects into the existing knowledge on the deposition of BCN films. First, we report on the deposition of thin BCN films at low substrate temperatures between 250 and 400 °C in purely thermal mode, and film characterization. A low temperature may promote the formation

of a single-phase BCN film. Triethylborane (TEB) and ammonia are used as the precursor and co-reactant, respectively. The presence of boron-to-carbon (B–C) bonds in the original TEB molecule increases the chance of the presence of B–C bonds in the final product, whereas NH_3 provides nitrogen atoms. The film growth occurs in a pulsed-deposition manner with purges in between, to limit the mechanism to merely surface reactions by mimicking an atomic layer deposition (ALD) process. Second, considering the rather low temperature budget, it is scientifically interesting to investigate to what extent ammonia is still able to react with (i.e., nitridize) a TEB-terminated surface at such low temperatures. Third, the role of gas pressure in the reactor, in view of the possible occurrence of a so-called surface-adduct assisted pathway,^{20–22} to enhance surface nitridation will be examined. Fourth, to increase the nitridation efficiency, we utilize the so-called hot wire (HW) assisted deposition in which molecular NH_3 dissociates into NH_2 radicals and atomic hydrogen (at-H) by using a hot tungsten wire kept at 1850 K.²³ Fifth, the (in)efficiency of carbon removal from the films at low temperatures, very relevant to the formation of BCN, will be the point of attention. Finally, we attempt to expand the range of materials from just BCN to AIBCN, by replacing selected TEB/ NH_3 cycles with trimethylaluminum (TMA) and NH_3 cycles, additionally incorporating aluminum. AIBCN films can presumably exhibit even larger tunability of their electrical and optical properties. If not explicitly specified in the text, abbreviations BCN and AIBCN neither denote any quantitative elemental composition nor represent any phase information.

II. EXPERIMENTAL

The BCN and AIBCN films were deposited in a home-built cluster deposition system described elsewhere.²³ Prior to deposition, Si (100) wafers underwent a three-step wafer cleaning procedure. This included (i) removal of native oxide by a 1-min dip into 1% HF, (ii) rinsing in deionized (DI) water, and (iii) ozone-steam cleaning followed by another HF dip and rinsing. The BCN films were deposited in the total pressure range of 0.2–10 mbar (regulated by a throttle valve), at substrate temperatures between 250 and 400 °C. The precursors were introduced via alternating pulses with Ar-purges in between, to avoid gas phase reactions. The precursor vessels were kept at 20 °C for both TEB and TMA precursors. The typical pulse- and purge durations were 0.5–2.0 s of TEB pulse (t_{TEB}), 0.5 s of TMA pulse (t_{TMA}), 5 s of Ar for post-TEB purge ($t_{\text{post-TEB}}$), 5 s of Ar for post-TMA purge ($t_{\text{post-TMA}}$), 2.0–60 s of NH_3 pulse (t_{NH_3}), and 2–80 s of Ar for post- NH_3 purge ($t_{\text{post-NH}_3}$). To realize AIBCN films by so-called super cycles, each TEB/Ar/ NH_3 /Ar cycle was followed by a TMA/Ar/ NH_3 /Ar cycle. The chosen pulse durations of the first sub-cycle were 0.5 s of TEB, 5 s of post-TEB purge, 30 s of t_{NH_3} , and 60 s of post- NH_3 purge. For the second sub-cycle, the durations were 0.5 s of TMA (t_{TMA}), 5 s of post-TMA purge, 10 s of t_{NH_3} , and 5 s of post- NH_3 purge.

In situ measurements of film thickness and film optical properties were carried out by a Woollam M2000UI spectroscopic ellipsometer (SE), operating in the wavelength range of 246–1689 nm (0.72–5.05 eV), in combination with CompleteEASE 5.19 modeling software. *Ex situ* SE measurements were performed with a Woollam M2000FI spectroscopic ellipsometer.

The validity of the SE analysis was verified by sensitivity tests, performed to confirm that the fits represented unique and global solutions rather than local or shallow minima, and to estimate errors in fitting the parameters. This resulted in calculating the mean square error (MSE) value, representing the agreement between the measured and modeled (fitted) data. A possible correlation between multiple fit parameters was minimized by variable angle SE (VASE) measurements (*ex situ*) and multi-sample analysis (MSA). The former provided more measurement events performed under different angles on the same location (spot) on the wafer. The MSA compared the same material at different film thicknesses, increasing the consistency in determining optical functions. To further verify the SE analysis, thicknesses of several selected samples were independently measured by high-resolution transmission electron microscopy (HRTEM) and x-ray reflectometry (XRR). The comparison indicated good agreement between the thickness values obtained from both SE, XRR and HRTEM, with a maximum deviation not exceeding 1–2 nm. This confirmed the applicability of the developed model and provided a solid platform for further characterization of the deposited films by SE.

The film composition was analyzed by x-ray photoelectron spectroscopy (XPS), with a Quantera SCM instrument using monochromatic Al K α radiation at 1486.6 eV. The C 1s peak due to ambient hydrocarbon contamination was calibrated at 284.8 eV.²⁴ Binding energies of the photoelectron lines of the film samples were charge-referenced to this C 1s line. For compositional analysis, XPS sputter depth profiling was performed using Ar ions. For each measurement point, the elemental composition was determined with an accuracy of 1–2 atomic percent (at. %). The stoichiometric coefficients, depicted in Figs. 3 and 7 and mentioned in the text, were the average values obtained for the particular layers from the corresponding XPS sputter profiles.

III. RESULTS AND DISCUSSION

A. Deposition of BCN films

Several experimental^{2–7,25} and theoretical^{1,26,27} works addressed the thermal decomposition of TEB and growth of BN films from TEB and NH_3 . Ethane (C_2H_6) elimination from a TEB: NH_3 adduct formed in the gas phase was proposed to occur through transitional states involving pre-formation of the adduct species, which could potentially evolve further and eventually form BN. However, overcoming the high energy barrier for C_2H_6 elimination might still be the limiting factor.¹ This energy barrier could be theoretically reduced by replacing one of the neighboring TEB: NH_3 adducts with a TMA: NH_3 adduct. Lowering the barrier would cause the formation of adduct-based transitional states more likely. Another expected reaction pathway might presumably involve the thermal decomposition of TEB at the growth surface.

Thermal decomposition of TEB starts at temperatures (T) exceeding 250 °C and is accompanied by releasing ethylene (C_2H_4) in Ar ambient and ethane in hydrogen (H_2) ambient.^{3,25,26,28} Above 400 °C, BH_3 formation is suggested via the elimination of the other two ethyl groups.^{26,28} Thus, one may expect an increased coverage of the growth surface with BH_3 -dissociation products at $T > 400$ °C. It should be noted that this process can hardly lead to a self-limiting ALD mode. Carbon incorporation into the films can originate from C_2H_4 or C_2H_2 since these hydrocarbons can enable carbon deposits

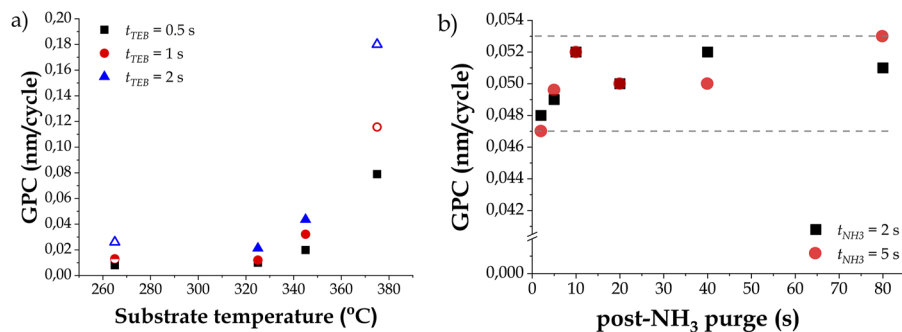


FIG. 1. (a) Variation of GPC as a function of T_S and t_{TEB} at a P_{tot} of 5 mbar. Other conditions: $t_{post-TEB} = 5$ s; t_{NH_3} is 5 s for the solid and open symbols and 2 s for the half-open symbols; $t_{post-NH_3}$ is 40 s for the solid and 10 s for open and half-open symbols. (b) Effect of t_{NH_3} and $t_{post-NH_3}$ on GPC at $P_{tot} = 5$ mbar. Between the horizontal dashed lines, the GPC varies within 0.006 nm/cycle.

at comparable temperatures.²⁵ The C₂H₂ can form via H₂ elimination from ethylene.^{26,29} Incorporation of C bonded to B may occur due to unbroken C–B bonds in the TEB fragments, assuming that there is no efficient chemical route to remove the carbon at low temperatures. (An example of such a route is the proposed removal of CH₃ groups from trimethylgallium (TMG) by the surface-adduct assisted pathway while forming gallium nitride (GaN) at 400 °C.)²² Chemisorption of NH₃ will be crucial to incorporate nitrogen. Since thermal dissociation of NH₃ occurs at high temperatures³⁰ ($T > 1000$ °C), lower shares of incorporated N can be expected within the temperature range of 300–400 °C investigated in this work. This low-temperature range is expected to lead to high B- and C-shares and a low N-share. Hence, utilizing a growth mechanism not involving direct NH₃-dissociation (e.g., surface-adduct based) can enhance the N-share.

1. Process kinetics

Figure 1(a) shows the effects of substrate temperature (T_S) and t_{TEB} on the growth rate per cycle (GPC). There are rather small changes in the GPC for $T_S < 325$ °C, whereas above this temperature, the GPC shows a sharp increase. This is likely due to the enhancement of thermal dissociation of TEB while approaching 375 °C.³ Since the GPC for the T_S ranging between 250 and 325 °C

remains nearly constant, one may speculate the occurrence of self-limiting surface reactions in this temperature range. From Fig. 1(b), one can see that the GPC is not significantly affected by both t_{NH_3} and $t_{post-NH_3}$. The analysis of the step-wise growth per cycle by *in situ* SE (not shown) revealed that $t_{post-NH_3}$ longer than 20 s is required to minimize possible gas phase reactions between TEB and NH₃ at a total pressure (P_{tot}) of 5 mbar. Increasing P_{tot} to 10 mbar requires at least 60 s of $t_{post-NH_3}$. Based on Fig. 1(a), t_{TEB} is fixed at 0.5 s for the subsequent experiments. Since temperatures below 325 °C reveal unpractically low GPC, to investigate the effect of T_S on the reaction with NH₃ and the removal of carbon, the range of 325–375 °C is further selected. From Fig. 1(a), there is presumably only a little decomposition of TEB at $T_S = 325$ °C, whereas $T_S = 375$ °C results in a significant decomposition.

Studying the influence of total pressure on GPC and layer composition is interesting, since it may suggest a possible contribution of the surface-adduct-assisted pathway to the film growth mechanism, as demonstrated earlier in our work for ALD of GaN films.²² In this work, no film growth was observed at P_{tot} of 10^{-3} mbar. From Fig. 2(a), the GPC noticeably increased, especially at $T_S = 375$ °C, with P_{tot} raising from 0.2 to 1 mbar, and remained rather unchanged for the pressure up to 5 mbar. At $T_S = 330$ °C, a further increase in

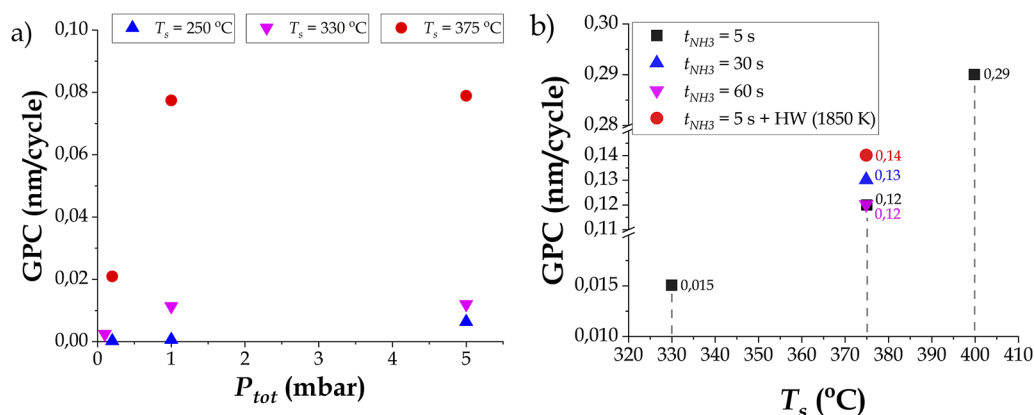


FIG. 2. (a) Variation of GPC as a function of P_{tot} (regulated by a throttle valve), T_S , and t_{NH_3} . Other conditions: $t_{TEB} = 0.5$ s, $t_{post-TEB} = 5$ s, $t_{NH_3} = 5$ s, and $t_{post-NH_3} = 40$ s. (b) GPC of samples deposited at various T_S and t_{NH_3} , as measured by *in situ* SE. The datapoint marked as “HW (1850 K)” corresponds to the attempt to dissociate molecular NH₃ into NH₂ radicals and atomic hydrogen by using a hot tungsten wire (HW) kept at 1850 K [see text below in relation to Fig. 3(b)]. Other process conditions can be found in Table S1 of the [supplementary material](#).

P_{tot} to 10 mbar resulted in a nearly constant GPC value of ~ 0.011 nm/cycle. At 250 °C, the GPC gradually increased with the pressure for all P_{tot} values. Deposition below the onset of thermal decomposition of TEB (250 °C) was impractical due to the very low GPC values.

Since longer t_{NH_3} may affect the efficiency of surface nitridation and thus cause a higher share of nitrogen in the layers, the influence of the NH_3 pulse time is investigated accordingly. From Fig. 2(b), the GPC is rather unaffected by changing t_{NH_3} in a wide range, similar to the other findings.^{4,31} This indicates that the shortest t_{NH_3} of 5 s is sufficient for completing surface reactions (or the reaction goes to an equilibrium state in 5 s).

2. Compositional analysis

XPS sputter-depth profile of a typical BCN sample is shown in Fig. 3(a), specifying the elemental shares from several samples summarized in Fig. 3(b). Remarkably, although obtained in the wide ranges of T_S and t_{NH_3} , the layers exhibit a nearly fixed composition of $B_{0.42}C_{0.41}N_{0.15}O_{0.02}$ with small variations within 1–2 at. %. This may indicate the formation of a single-phase material, since assuming the co-synthesis of separate (BN_x , BC_y , CN_z , etc.) phases with their fixed ratio in such a wide range of conditions seems rather unusual. Varying T_S only influenced the GPC [recall Figs. 1(a) and 2(b)], hardly affecting the composition.

The attempt to dissociate molecular NH_3 into NH_2 radicals and atomic hydrogen (at-H) by using a hot wire (HW),²³ thereby incorporating more nitrogen into the layers, led to the opposite effect. In fact, the amount of nitrogen decreased from 15 to 6 at. %, accompanied by an increase in the B- and, in particular, C-shares [Fig. 3(b)]. This suggests that the removal of carbon from the layers occurs via the incorporation of nitrogen: a higher N-share leads to a lower C-share and vice versa. Alternatively, the presence of at-H can suppress the removal of carbon. In this light, an altered surface chemistry to explain similar observations is proposed.³² Since at-H can promote the decomposition of hydrocarbons, this may enhance the deposition of carbon. The attempt to increase N incorporation by elongating t_{NH_3} slightly influenced the elemental ratio [see last three rows in Fig. 3(b)]. This confirmed that time was not the limiting factor, at least not at $T_S = 375$ °C. The fact that the three bottom samples have the same C-share but somewhat different N-shares can

be attributed to the partial replacement of N by O, reducing the N-share.

The XPS analysis of chemical bonding environments was further performed to clarify whether the as-obtained $B_{0.42}C_{0.41}N_{0.15}O_{0.02}$ stoichiometry could be interpreted as a single-phase material or a mixture of separate phases. Figure 4 shows representative peak fitting of the B 1s, C 1s, and N 1s peaks. Gaussian fitting is performed after fixing the peak positions at the corresponding values, in accordance with the studies referred to in Tables S2 and S3. For the samples of Fig. 3(b), there is no apparent shift detected for the B 1s and C 1s peaks with neither varying T_S or t_{NH_3} nor applying the HW assistance. The B 1s peak is observed at ~ 189.6 eV, and the fits suggest three possible chemical states of boron (neglecting the B–O subpeak) centered at 187.6, 189.4, and 190.6 eV [Fig. 4(a)]. Three subpeaks are needed to adequately describe the C 1s spectra [Fig. 4(b)]. The N 1s spectrum is found to have a tail toward higher binding energies, when a longer t_{NH_3} is used (see Fig. S1 in the supplementary material), indicating a change in the bonding environment. The subpeak located at 399.3 eV can be assigned to C–N bonding (presumably in sp^3 C–N binding state),^{33,34} whereas the peak located at 400.3 eV can occur due to C–N bonding (sp^2 C–N or C=N binding state) according to the reports summarized in Ref. 35. See also other references in Tables S2 and S3 in relation to the peak assignment.

The XPS analysis can suggest at least two bonding environments for N and three for C and B (neglecting the B–O subpeak). The presence of a single BC_xN_y phase can be speculated, however, not excluding the formation of separate BC_x , CN_y , pure-C, and BN phases. As mentioned above, the elemental composition, only slightly varying around $B_{0.42}C_{0.41}N_{0.15}O_{0.02}$ for T_S of 330–400 °C and t_{NH_3} of 5–60 s [Fig. 3(b)], may additionally point to the formation of a single-phase BCN. A further investigation with additional analysis techniques is required to better identify the available phases; however, this is not in the scope of this work.

3. Optical properties

To calculate the refractive index (n) of the BCN films from SE, the B-spline model was used. If the material was assumed to be transparent in the range of 0–2.48 eV, i.e., the B-spline model was replaced by the Cauchy model, this only affected the values of

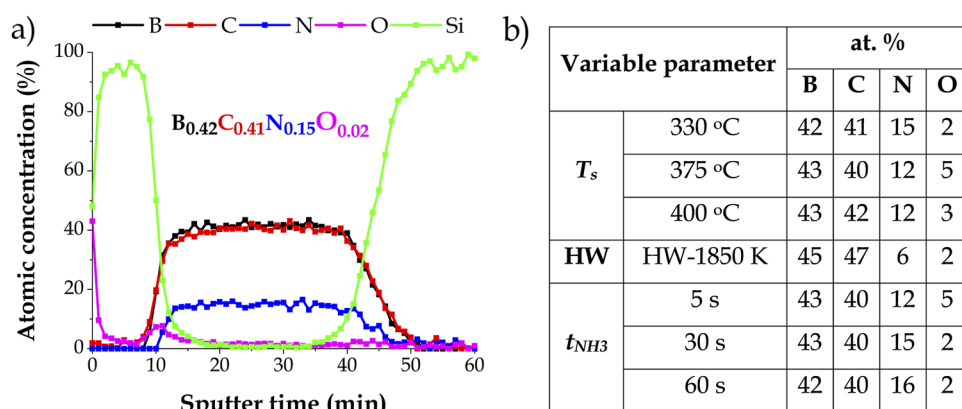


FIG. 3. (a) XPS sputter-depth profile of a representative $B_{0.42}C_{0.41}N_{0.15}O_{0.02}$ sample capped with an amorphous silicon (a-Si) layer to prevent film oxidation in the air. To be noted: the given stoichiometry does not necessarily imply a single-phase material. (b) Shares of various elements (in at. %) for samples deposited at different T_S and t_{NH_3} . Row "HW-1850 K" corresponds to the attempt to dissociate molecular NH_3 into NH_2 radicals and atomic hydrogen by using an HW kept at 1850 K. Other deposition conditions can be found in Table S1.

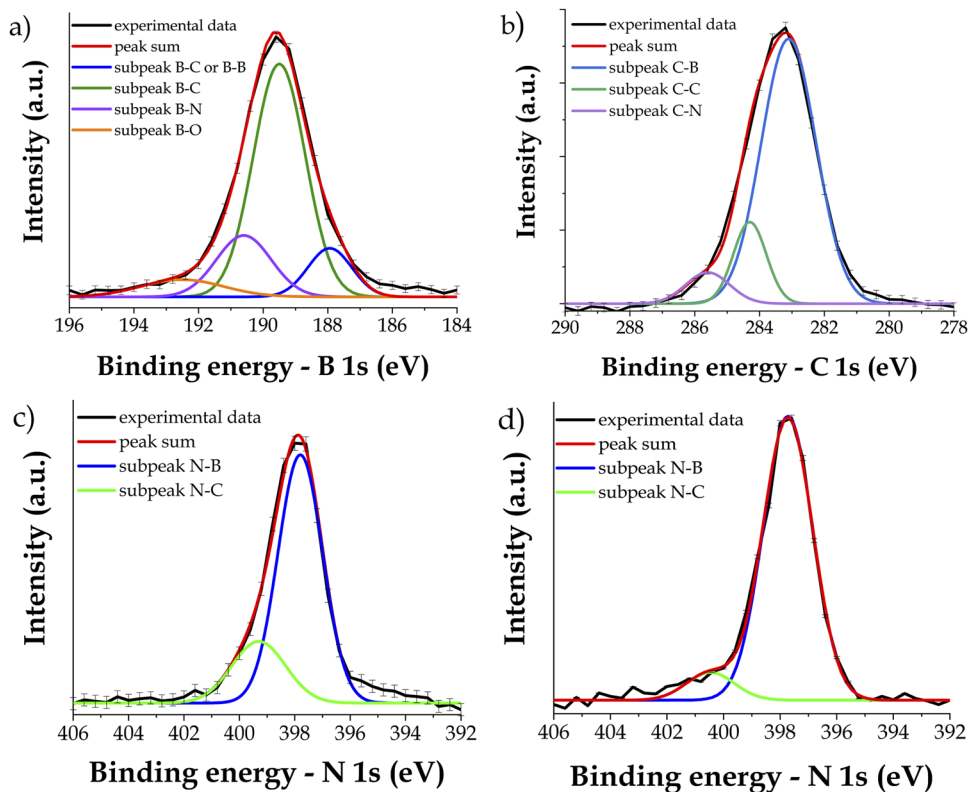


FIG. 4. Multi-peak fitting of representative XPS peaks of a $B_{0.42}C_{0.41}N_{0.15}O_{0.02}$ film for (a) B 1s, (b) C 1s, and (c) and (d) N 1s peaks with and without HW-assistance, respectively. To be noted: for the film deposited at the longest t_{NH_3} of 60 s, a shift toward higher binding energies is observed in the N 1s spectra (see Fig. S1).

n within a few percent (the actual error margin of the measurements). To evaluate the extinction coefficient (k), an attempt was made with the B-spline model as well, giving the values of k varying between 0.1 and 0.15, likely due to the presence of C. Still, the behavior of k we obtained was unclear and should be verified further, requiring additional experimentation and time-consuming model development, both left out of this work.

The as-calculated n is plotted in Fig. 5. From Fig. 5(a), there is no significant effect of T_S on n . This can be expected from the similar elemental composition shown in Fig. 3(b). A slight increase in n in the case of the HW assistance is possibly due to the somewhat higher share of C in the films or a small increase in their density. Changing the ammonia pulse duration has a larger effect: n decreases with elongating t_{NH_3} [Fig. 5(b)]. The averaged composition from XPS [Fig. 3(b)] exhibits only 3–4 at. % higher N-content for longer times. However, such small compositional changes can still influence n . For example, a decrease in n by ~6%, if changing the composition from $B_{0.1}C_{0.55}N_{0.35}$ to $B_{0.13}C_{0.54}N_{0.33}$ and further to $B_{0.14}C_{0.51}N_{0.35}$ stoichiometry, is mentioned.³⁴ The effect is attributed to the increased share of B–N and C–N bonds in the compound. Other works mention a decrease in the optical bandgap of samples containing 13 at. % of C, presumably due to the incorporation of C atoms into the amorphous region of BCN films, forming C=C and C=N bonds.^{9,36} The occurrence of a 15% larger bandgap for samples with similar composition is further reported,⁸ attributed to changes in the chemical bonding network. Narrowing the bandgap is reported for amorphous C:H films with decreasing H content.^{37–39}

We propose that both elemental composition and chemical bonding environment play a role in the ~10% change in the refractive index seen in Fig. 5(b). The films that experienced longer NH_3 pulses exhibit lower n . From Fig. S1, the $B_{0.42}C_{0.40}N_{0.16}O_{0.02}$ film deposited at $t_{NH_3} = 60$ s (last row in Fig. 3(b)) exhibits the N 1s peak position at ~400.4 eV, whereas the $B_{0.43}C_{0.40}N_{0.12}O_{0.05}$ film obtained at $t_{NH_3} = 5$ s [third row from the bottom in Fig. 3(b)] shows the position at ~399.3 eV. According to Table S2, the lower binding energy may correspond to sp^3C-N binding state,^{33,34} whereas the higher binding energy can be attributed to sp^2C-N binding state or C=N bonding.³⁵ Changing the binding state together with the increased N-share is assumed to result in the observed 10% decrease in n for the longer t_{NH_3} .

B. AIBCN films obtained by super-cycles

As mentioned in Sec. III A, TEB: NH_3 adduct may be considered as a transitional state, which can potentially evolve further and eventually form BN. Overcoming the high energy barrier for by-product elimination may be the limiting factor there.¹ This energy barrier can be theoretically reduced by replacing one of the neighboring TEB: NH_3 adducts with a TMA: NH_3 adduct. In this view, the realization of super-cycles in which each TEB/Ar/ NH_3 /Ar cycle is followed by a TMA/Ar/ NH_3 /Ar cycle, to form an AIBCN film, is scientifically appealing.

Although a t_{NH_3} value of 5 s seemed to be sufficient for the GPC of the BCN films to saturate [recall Fig. 1(b)], we still used the

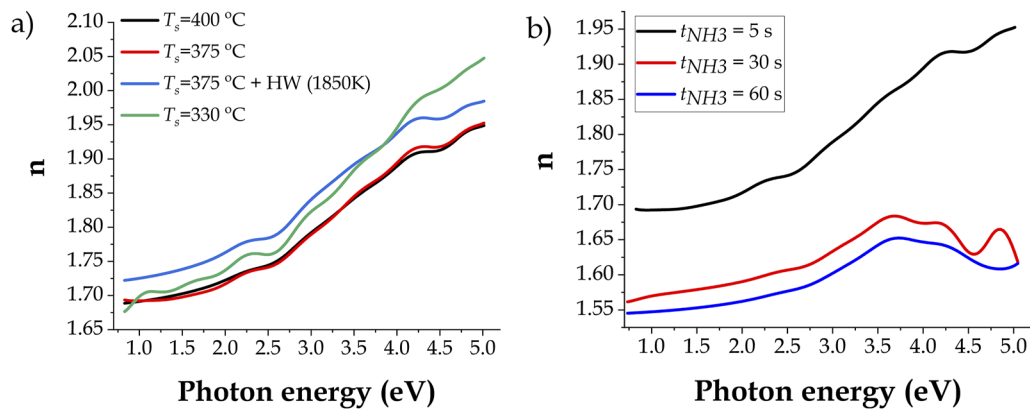


FIG. 5. Refractive index n of the films of Fig. 3(b) deposited at various (a) T_S and (b) t_{NH_3} . Other process conditions can be found in Table S1.

longer t_{NH_3} for the AIBCN films to ensure that the nitridation reaction occurred as much as possible. To investigate the total pressure effect, the films were deposited at a P_{tot} of either 0.2 or 10 mbar.

1. Deposition kinetics

At a P_{tot} of 0.2 mbar, a GPC of 0.1 nm/cycle is obtained. Considering that the GPC of a BCN film is only 0.02 nm/cycle at this pressure [refer to Fig. 2(a)], the GPC of 0.1 nm/cycle may indicate the dominant deposition of AlN. On the other hand, at a P_{tot} of 10 mbar, BCN films can easily grow, suggesting the incorporation of a larger share of BCN into the AIBCN material. Furthermore, the deposition at 10 mbar is found to be thickness dependent. For example, a GPC of 0.11 nm/cycle was obtained for the thicknesses up to ~10 nm, which further increased to 0.14 nm/cycle above this thickness (see Fig. S2). Speculatively, this could be explained by closing (i.e., reaching full surface coverage) the film above the 10-nm critical thickness. (To be noted: films grown at $P_{tot} = 0.2$ mbar were, due to their low GPC, all thinner or just comparable with this critical thickness, so the effect remained unidentified at low pressures.)

The shape evolution of individual precursor cycles, measured by SE, is analyzed further. However, before proceeding, let us

emphasize the following. The extremely small variations of the SE signal within a cycle are interpreted by the SE optical model as thickness variations. Apart from this, changing the surface optical properties upon the corresponding chemical reactions may also influence the signal. One should bear in mind that only the start and end points of each cycle can be attributed to the real thickness values as they compose the entire (linear) growth curve. Since the final film thickness can be verified by alternative measurement techniques (electron microscopy, x-ray reflection, etc.), the positions of the start and end points of each cycle on the growth curve can be reliably determined. However, this cannot be straightforwardly applied to the thickness variations between these points.

Still assuming that the thickness variation within a cycle, as shown in Fig. 6, is a real phenomenon, the following analysis is worth applying. At 0.2 mbar, the first strong up-step of a cycle [Fig. 6(a)] corresponds to the introduction of TMA and presumably indicates its successful chemisorption. The subsequent introduction of ammonia leads to a small down-step. The next TEB pulse causes a weak increase in the “thickness.” This may be expected considering the low GPC of BCN at 0.2 mbar [Fig. 2(a)], much lower than the GPC of AlN (~0.1 nm/cycle from our experiments) at the same

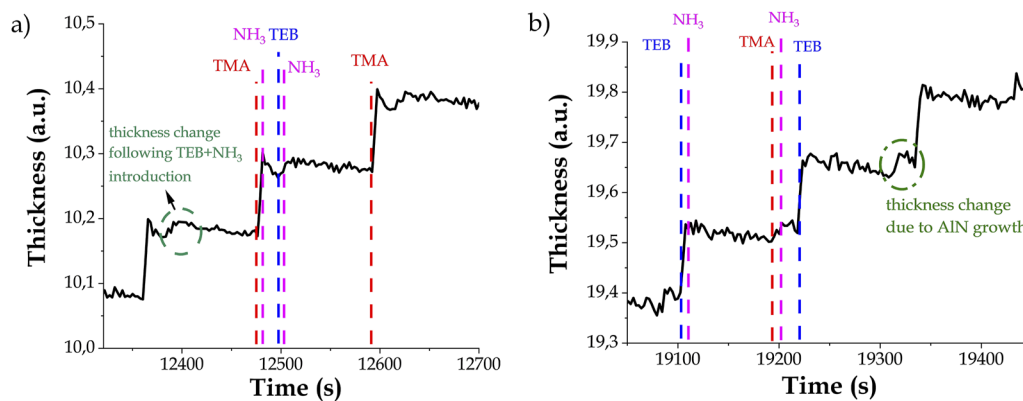


FIG. 6. Step-shape comparison for deposition at $T_S = 375$ °C and P_{tot} of (a) 0.2 mbar or (b) 10 mbar.

temperature and pressure. Therefore, the pulse-shape analysis may already suggest the dominant growth of AlN with a little addition of BCN at $P_{tot} = 0.2$ mbar. At $P_{tot} = 10$ mbar, the kinetics seems to reverse, showing only a small “thickness” increase after each TMA pulse and a large up-step after each TEB pulse [Fig. 6(b)]. This may suggest that the chemisorption of TMA on a surface containing chemisorbed TEB species is inhibited, leading to the dominant growth of BCN with a little share of AlN. The compositional analysis below confirms this.

2. Compositional analysis

The XPS sputter-depth profiling is shown in Fig. 7. Apart from Al, B, C, and N, low amounts of oxygen (less than 5 at. %) can be seen. For deposition at a P_{tot} of 0.2 mbar, about 34 at. % of Al is incorporated into the film [Fig. 7(a)]. This is in line with the observations for the kinetics and can be explained by the demonstrated inhibited growth of BCN at such a low pressure. For deposition at a P_{tot} of 10 mbar, the layer mainly consists of B, C, and N, with ~2 at. % of Al [Fig. 7(b)]. Here, the BCN deposition takes over the AlN deposition, somehow preventing the involvement of TMA molecules in the film growth. Similarly, boron and/or carbon can occupy the active surface sites, preventing the chemisorption of TMA.

Figure S3 shows the multi-peak fitting of Al 2p, B 1s, and N 1s XPS peaks of the sample of Fig. 7(a) by using Gaussian fitting based on the positions of the subpeaks fixed according to Table S3. The C 1s peak (not shown in Fig. S3 due to its low intensity being near the detection limit—no multi-peak fitting performed) position shifted toward lower energies, namely to 282.0 eV, possibly due to the presence of Al. Nitrogen shows two different bonding states attributed to N–Al and N–B bonds as in AlN and BN, respectively. The weak nitrogen–carbon subpeak, presumably present at ~399 eV, can be assigned to C–N bonding (see Table S3 and corresponding references). From the measured stoichiometry and the sub-peak analysis, one may speculate that the $\text{Al}_{0.34}\text{B}_{0.13}\text{C}_{0.03}\text{N}_{0.49}\text{O}_{0.01}$ sample of Fig. 7(a) obtained at $P_{tot} = 0.2$ mbar contains mixed AlN and BN phases.

Figure S4 shows the multi-peak fitting of the $\text{Al}_{0.02}\text{B}_{0.41}\text{C}_{0.36}\text{N}_{0.15}\text{O}_{0.06}$ sample of Fig. 7(b) deposited at $P_{tot} = 10$ mbar. The B 1s and C 1s spectra exhibit bonding states located at binding energies similar to those of the $\text{B}_{0.42}\text{C}_{0.41}\text{N}_{0.15}\text{O}_{0.02}$ film of Fig. 4. Furthermore, the Al 2p peak can be successfully fitted by the two subpeaks attributed to AlN and Al_2O_3 , similar to the 0.2-mbar sample. The

N 1s peak shows two different bonding states attributed to N–Al and N–B bonds as in AlN and BN, respectively. In addition, from the multi-peak fitting of the N 1s peak, a weak subpeak due to C–N bonding may be suggested. The peak position ranges between 399.0 and 400.3 eV, depending on the vertical position through the film thickness probed by XPS. At the film surface, this C–N peak appears at 399.0 eV, whereas it shifts to 400.3 eV while approaching the film/substrate interface. This shift can occur due to a change in the bonding environment of nitrogen, which can further cause the GPC to increase above the 10-nm film thickness (see Fig. S2). The N 1s subpeak at 399.0 can be assigned to C–N bonding, whereas the 400.3-eV subpeak to C–N or C=N bonding.^{33–35} One may refer to Tables S2 and S3 for further details regarding the peak positions and corresponding references.

In terms of its composition and chemical bonding environments from XPS, the $\text{Al}_{0.02}\text{B}_{0.41}\text{C}_{0.36}\text{N}_{0.15}\text{O}_{0.06}$ sample resembles the $\text{B}_{0.42}\text{C}_{0.41}\text{N}_{0.15}\text{O}_{0.02}$ sample of Figs. 3 and 4. As for the optical properties (see Fig. S5), the refractive index of the film deposited at $P_{tot} = 0.2$ mbar is close to that of pure AlN,⁴⁰ deviating by ~10%, which can be attributed to the low-level inclusions of boron and carbon. At $P_{tot} = 10$ mbar, a significantly lower n is obtained, caused by the large share of $\text{B}_{0.42}\text{C}_{0.41}\text{N}_{0.15}\text{O}_{0.02}$, in agreement with Fig. 5.

IV. SUMMARY AND CONCLUSIONS

This work aimed to bring several novel insights into the existing knowledge on the deposition of (Al)BCN films in the low-temperature range of 250–400 °C from TEB (plus optionally TMA) and NH_3 , in line with the six scientific questions posed in the introduction. The XPS analysis suggested at least two bonding environments for N and three for C and B. From this, the presence of the single BC_xN_y phase can be speculated, not excluding the formation of separate BC_x , CN_y , pure-C, and BN phases. However, the nearly similar elemental composition of $\text{B}_{0.42}\text{C}_{0.41}\text{N}_{0.15}\text{O}_{0.02}$, varied only within 1–2 at. % for the substantial ranges of substrate temperature (from 330 °C and up to 400 °C) and NH_3 -exposure time (t_{NH_3} of 5–60 s) changes, might indicate a similar growth mechanism and formation of the material with single phase. In other words, applying a low thermal budget could beneficially promote the formation of this single-phase BCN material.

From XPS, applying the longest t_{NH_3} influenced the N 1s bonding environment. The lower binding energy of 399.3 eV might correspond to the $\text{sp}^3\text{C–N}$ binding state, whereas the higher binding

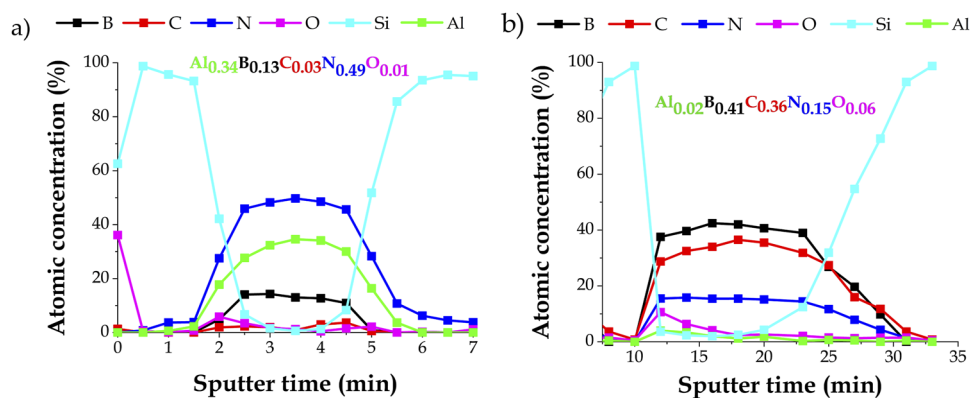


FIG. 7. XPS sputter-depth profiles of (Al)BCN samples (capped with a-Si layer) deposited at $T_S = 375$ °C and P_{tot} of (a) 0.2 mbar or (b) 10 mbar. The indicated stoichiometric coefficients are calculated from the peak-intensity ratios and do not necessarily imply the occurrence of a single-phase material.

energy of 400.4 eV could be attributed to the sp^2C-N binding state or $C=N$ bonding. In addition, the N-share increased by 3–4 at. %. As a result, the refractive index of the BCN material decreased by ~10%.

In the range of T_S between 265 and 325 °C, the GPC of BCN remained nearly constant. This might suggest the occurrence of self-limiting surface reactions. Furthermore, the remarkable dependence of GPC on the total pressure, approaching a near saturation regime between 1 and 10 mbar for both $T_S = 330$ °C and $T_S = 375$ °C, might also indicate the occurrence of a pressure-independent surface coverage or self-limiting surface reactions at these pressures. The coverage, and therefore the reactions, were however dependent on the T_S . One should bear in mind that the GPC-saturation behavior could not be explained by underdosing the precursor, since just elevating the temperature from 330 to 375 °C in the saturation region, while keeping the same precursor dose, significantly increased the GPC.

The GPC-vs- P_{tot} behavior might support the occurrence of the surface-adduct assisted pathway in the film growth mechanism since it showed a similar trend as reported in our earlier work on thermal ALD of GaN films.²² Briefly, the purely thermal ALD of GaN occurred between 375 and 425 °C and yielded a GPC as high as 0.1 nm/cycle. Carbon-free, polycrystalline films with sub-10 nm crystalline domains were deposited. The approach relied on the speculated existence of the so-called trimethylgallium-ammonia (TMG:NH₃) surface adduct, and its conversion into GaN network. Importantly, the formation of the surface adduct might be strongly enhanced by the partial pressure of NH₃, whereas its conversion was enhanced by the duration of NH₃ pulses.

In this work, in the T_S range of 330–375 °C, the GPC also noticeably increased with increasing P_{tot} to 1 mbar and remained unchanged for the pressure up to 10 mbar. However, the level of saturation of the GPC was influenced by T_S , which is very similar to the effect observed in Ref. 22. (One should once again bear in mind that underdosing of the precursor was excluded.) From these results, the existence of a TEB:NH₃ surface adduct might be speculated.

Considering the low thermal budget used in this work, it was scientifically interesting to investigate to what extent NH₃ was able to react with a TEB-terminated surface, providing its nitridation. It appeared that, in the ranges of temperatures and NH₃-exposure times applied, the N-share varied within 12–16 at. % only. This suggested a limited reactivity of NH₃ with the surface. Once again, the narrow range of the N-share variation, while significantly changing both temperature and pressure, might point to a similar deposition mechanism and the formation of a single-phase material. The same argument holds for the C-share, nearly fixed at 40–42 at. %. This means that the removal of carbon from the films was hardly affected by both temperature and pressure.

The work further attempted to increase the nitrogen share in the layers by dissociating molecular NH₃ into NH₂ radicals via implementing hot wire assistance. This remarkably led to the opposite effect, i.e., the amount of nitrogen decreased from ~15 to 6 at. %, yielding a composition of B_{0.45}C_{0.47}N_{0.06}O_{0.02} instead of B_{0.42}C_{0.41}N_{0.15}O_{0.02}. The decrease in the nitrogen share was accompanied by a corresponding increase in the B- and, in particular, C-shares. The latter suggested that the removal of carbon might occur via the incorporation of nitrogen—another argument in the favor of the formation of the single-phase BCN material.

As for the AIBCN films, a P_{tot} of 10 mbar resulted in ~10% higher GPC, as compared to that at a P_{tot} of 0.2 mbar. Furthermore, changing P_{tot} had a strong impact on the film's elemental composition. Al_{0.34}B_{0.13}C_{0.03}N_{0.49}O_{0.01} and Al_{0.02}B_{0.41}C_{0.36}N_{0.15}O_{0.06} films were grown at 0.2 and 10 mbar, respectively. This indicated that the enhanced BCN deposition occurred at $P_{tot} = 10$ mbar, whereas at $P_{tot} = 0.2$ mbar, the films largely consisted of AlN. In terms of the refractive index, composition, and chemical bonding environments, the Al_{0.02}B_{0.41}C_{0.36}N_{0.15}O_{0.06} films grown with super-cycles resembled the B_{0.42}C_{0.41}N_{0.15}O_{0.02} samples obtained without super-cycles. In the Al_{0.34}B_{0.13}C_{0.03}N_{0.49}O_{0.01} films grown at $P_{tot} = 0.2$ mbar, the co-existence of stoichiometric AlN and BN phases might be suggested.

SUPPLEMENTARY MATERIAL

Additional information on deposition and characterization details of (Al)BCN films, given in Figs. S1–S5 and Tables S1–S3, can be found in the [supplementary material](#).

ACKNOWLEDGMENTS

This work has been financially supported by The Netherlands Organization for Scientific Research (NWO), Domain Applied and Engineering Sciences (TTW) (Project No. 13929). The authors thank G. A. M. Kip, MESA+ Institute, for the XPS measurements. They also thank R. A. M. Wolters and J. Schmitz, University of Twente, for the fruitful discussions. The authors acknowledge Toyota Europe and ASM International for their partial financial support of Project No. 13929.

AUTHOR DECLARATIONS

Conflict of Interest

The authors have no conflicts to disclose.

Author Contributions

Ramazan O. Apaydin: Conceptualization (equal); Data curation (equal); Formal analysis (equal); Investigation (equal); Writing – original draft (equal). **Antonius A. I. Aarnink:** Investigation (equal); Methodology (equal). **Dirk J. Gravesteijn:** Supervision (equal); Writing – review & editing (equal). **Michel P. de Jong:** Funding acquisition (equal); Supervision (equal); Writing – review & editing (equal). **Alexey Y. Kovalgin:** Conceptualization (equal); Funding acquisition (equal); Project administration (lead); Supervision (lead); Writing – review & editing (equal).

DATA AVAILABILITY

The data that support the findings of this study are available within the article and its [supplementary material](#).

REFERENCES

- R. R. Q. Freitas, G. K. Gueorguiev, F. De Brito Mota, C. M. C. De Castilho, S. Stafström, and A. Kakanakova-Georgieva, *Chem. Phys. Lett.* **583**, 119 (2013).
- M. Imam, C. Höglund, S. Schmidt, R. Hall-Wilton, J. Birch, and H. Pedersen, *J. Chem. Phys.* **148**, 034701 (2018).
- A. Haider, C. Ozgüt-Akgun, E. Goldenberg, A. K. Okyay, and N. Biyikli, *J. Am. Ceram. Soc.* **97**, 4052 (2014).

- ⁴M. Snure, Q. Paduano, M. Hamilton, J. Shoaf, and J. M. Mann, *Thin Solid Films* **571**, 51 (2014).
- ⁵O. J. Kilbury, K. S. Barrett, X. Fu, J. Yin, D. S. Dinair, C. J. Gump, A. W. Weimer, and D. M. King, *Powder Technol.* **221**, 26 (2012).
- ⁶W. Hao, C. Marichy, and C. Journet, *2D Mater.* **6**, 012001 (2019).
- ⁷S. Joh and G. H. Evans, in *Proceedings of the 13rd International Conference on Chemical Vapor Deposition*, edited by T. M. Besmann, M. D. Allendorf, M. Robinson, and R. K. Ulrich (Electrochemical Society, NJ, 1996), pp. 588–593.
- ⁸A. Prakash and K. B. Sundaram, *Appl. Surf. Sci.* **396**, 484 (2017).
- ⁹H. Sota, C. Kimura, H. Aoki, and T. Sugino, *Diamond Relat. Mater.* **19**, 1441 (2010).
- ¹⁰H. Moreno Fernández, D. Rogler, G. Sauthier, M. Thomasset, R. Dietsch, V. Carlino, and E. Pellegrin, *Sci. Rep.* **8**, 1293 (2018).
- ¹¹E. A. Il'inchik, V. V. Volkov, and L. N. Mazalov, *J. Struct. Chem.* **46**, 523 (2005).
- ¹²M. A. Mannan, M. Nagano, K. Shigezumi, T. Kida, N. Hirao, and Y. Baba, *Am. J. Appl. Sci.* **5**, 736 (2008).
- ¹³M. O. Watanabe, T. Sasaki, S. Itoh, and K. Mizushima, *Thin Solid Films* **281–282**, 334 (1996).
- ¹⁴H. Künzli, P. Gantenbein, R. Steiner, and P. Oelhafen, *J. Anal. Chem.* **346**, 41 (1993).
- ¹⁵A. Perrone, A. P. Caricato, A. Luches, M. Dinescu, C. Ghica, V. Sandu, and A. Andrei, *Appl. Surf. Sci.* **133**, 239 (1998).
- ¹⁶V. S. Sulyaeva, Y. M. Rumyantsev, V. G. Kesler, and M. L. Kosinova, *Thin Solid Films* **581**, 59 (2015).
- ¹⁷T. Thamm, D. Wett, W. Bohne, E. Strub, J. Röhrich, R. Szargan, G. Marx, and W. A. Goedel, *Microchim. Acta* **156**, 53 (2006).
- ¹⁸V. O. Todi and K. B. Sundaram, *Electrochem. Solid-State Lett.* **14**, G49 (2011).
- ¹⁹A. R. Burke, C. R. Brown, W. C. Bowling, J. E. Glaub, D. Kapsch, C. M. Love, R. B. Whitaker, and W. E. Moddeman, *Surf. Interface Anal.* **11**, 353 (1988).
- ²⁰T. M. Mayer, J. W. Rogers, Jr., and T. A. Michalske, *Chem. Mater.* **3**, 641 (1991).
- ²¹M. E. Bartram, T. A. Michalske, J. W. Rogers, Jr., and R. T. Paine, *Chem. Mater.* **5**, 1424 (1993).
- ²²S. Banerjee, A. A. I. Aarnink, D. J. Gravesteijn, and A. Y. Kovalgin, *J. Phys. Chem. C* **123**, 23214 (2019).
- ²³A. Y. Kovalgin, M. Yang, S. Banerjee, R. O. Apaydin, A. A. I. Aarnink, S. Kinge, and R. A. M. Wolters, *Adv. Mater. Interfaces* **4**, 170005 (2017).
- ²⁴T. L. Barr and S. Seal, *J. Vac. Sci. Technol., A* **13**, 1239 (2002).
- ²⁵J. S. Lewis, S. Vaidyaraman, W. J. Lackey, P. K. Agrawal, G. B. Freeman, and E. K. Barefield, *Mater. Lett.* **27**, 327 (1996).
- ²⁶M. Imam, K. Gaul, A. Stegmüller, C. Höglund, J. Jensen, L. Hultman, J. Birch, R. Tonner, and H. Pedersen, *J. Mater. Chem. C* **3**, 10898 (2015).
- ²⁷M. Imam, *CVD Chemistry of Organoborons for Boron–Carbon Thin Film Depositions* (Linköping University, 2017).
- ²⁸H. Pedersen, C. Höglund, J. Birch, J. Jensen, and A. Henry, *Chem. Vap. Deposition* **18**, 221 (2012).
- ²⁹C. D. Stinespring and J. C. Wormhoudt, *J. Cryst. Growth* **87**, 481 (1988).
- ³⁰S. S. Liu and D. A. Stevenson, *J. Electrochem. Soc.* **125**, 1161 (1978).
- ³¹D. Jin-Xiang, Z. Xiao-Kang, Y. Qian, W. Xu-Yang, C. Guang-Hua, and H. De-Yan, *Chin. Phys. B* **18**, 4013 (2009).
- ³²M. Chubarov, H. Pedersen, H. Höglberg, J. Jensen, and A. Henry, *Cryst. Growth Des.* **12**, 3215 (2012).
- ³³F. Zhou, K. Adachi, and K. Kato, *Thin Solid Films* **497**, 210 (2006).
- ³⁴M. K. Lei, Q. Li, Z. F. Zhou, I. Bello, C. S. Lee, and S. T. Lee, *Thin Solid Films* **389**, 194 (2001).
- ³⁵E. D'Anna, M. L. De Giorgi, A. Luches, M. Martino, A. Perrone, and A. Zocco, *Thin Solid Films* **347**, 72 (1999).
- ³⁶C. Kimura, H. Sota, H. Aoki, and T. Sugino, *Diamond Relat. Mater.* **18**, 478 (2009).
- ³⁷J. C. Angus and C. C. Hayman, *Science* **241**, 913 (1988).
- ³⁸B. Dischler, A. Bubenzer, and P. Koidl, *Appl. Phys. Lett.* **42**, 636 (1983).
- ³⁹J. Robertson and E. P. O'Reilly, *Phys. Rev. B* **35**, 2946 (1987).
- ⁴⁰S. Banerjee, *From Radical-Enhanced to Pure Thermal ALD of Aluminium and Gallium Nitrides* (University of Twente, Enschede, The Netherlands, 2019).